Construction and Building Materials 245 (2020) 118384

Contents lists available at ScienceDirect

Construction and Building Materials

journal homepage: www.elsevier.com/locate/conbuildmat

Experimental investigation of ASR-affected concrete – The influence of uniaxial loading on the evolution of mechanical properties, expansion and damage indices

Simen Sørgaard Kongshaug [a,b,*], Oddbjørn Oseland [b], Terje Kanstad [b], Max A.N. Hendriks [b,c], Eva Rodum [d], Gro Markeset [a]

[a] Oslo Metropolitan University, Pilestredet 35, 0130 Oslo, Norway
[b] Norwegian University of Science and Technology, Richard Birkelandsvei 1A, 7034 Trondheim, Norway
[c] Delft University of Technology, Stevinweg 1, 2628 CN Delft, The Netherlands
[d] Norwegian Public Roads Administration, Abels Gate 5, 7030 Trondheim, Norway

HIGHLIGHTS

- Uniaxial sustained stress reduce the volumetric expansion due to ASR.
- No transfer of expansion to unrestrained directions was observed.
- Damage due to ASR is most notable from the reduction of modulus of elasticity.
- Modulus of elasticity decreases with increasing levels of expansion.

ARTICLE INFO

Article history:
Received 8 July 2019
Received in revised form 4 February 2020
Accepted 7 February 2020
Available online 19 February 2020

Keywords:
Concrete
Alkali-silica reaction
Expansion
Degradation
Stiffness damage test
Mechanical properties
Uniaxial sustained loading

ABSTRACT

The alkali silica reaction (ASR) in concrete causes internal localized swelling and micro cracking, which result in expansion and correlated deterioration of the concrete material. The stress state of the concrete is known to affect expansion due to ASR, with an anisotropic stress state giving rise to anisotropic expansion. Similarly, the orientation and extent of micro cracking have a directional effect on the concrete mechanical behaviour. This research studied the effect of sustained uniaxial compressive stress on the evolution of the mechanical behaviour of concrete in compression. Concrete cubes of 230 mm side length were uniaxially restrained and stored in accelerated conditions, with cores drilled in two directions for mechanical tests: a cyclic test in compression, i.e. a stiffness damage test (SDT) and a complete stress-strain test. A clear directional dependency of the mechanical characteristics was found. Furthermore, the results indicate that reduction in modulus of elasticity is well correlated with the expansion in the test direction. On the other hand, the damage indices obtained from the SDT merely relate to the expansion, which puts in question the SDT's ability to predict ASR expansion in stressed concrete and therefore in concrete structures.

1. Introduction

Alkali-silica reaction (ASR) in concrete is a chemical reaction between alkalis mostly from the cement paste, and silica from reactive aggregates. The product of the reaction is a hydrophilic gel that swells by water absorption. Pressure develops in the ASR gel and causes tensile stresses in the surrounding material. Consequently, micro cracks develop in a diffuse pattern. The effect of ASR on the concrete is expansion (strains) and degradation of material properties like stiffness and strength [1,2]. Furthermore, experiments show the stress state affects the expansion, i.e. ASR-induced strains are reduced in the compressed directions [3–7]. The expansion is related to the degree and orientation of the micro cracking in the material, which result in anisotropic material behaviour in terms of stiffness and strength. Barbosa et al. [8] studied the influence of the ASR-induced crack orientation on the compressive strength and modulus of elasticity of drilled cores from ASR-damaged slab bridges. They concluded that the

* Corresponding author at: Oslo Metropolitan University, Pilestredet 35, 0130 Oslo, Norway.
E-mail address: simkon@oslomet.no (S.S. Kongshaug).

https://doi.org/10.1016/j.conbuildmat.2020.118384
0950-0618/

compressive strength and the stiffness were lower in the direction perpendicular to the cracks than in the direction parallel to the cracks. Giaccio et al. [9] found the same trend in laboratory cast cylinders exposed to accelerated ASR conditions and uniaxial sustained loading, i.e. higher stiffness and compressive strength were found in specimens with cracks oriented in the loading direction. Gautam et al. [10] carried out mechanical testing on cores that were drilled from cubes exposed to various stress states under accelerated ASR conditions. They found that the expansion, cracking and change in stiffness of concrete showed directional behaviour with the stress state. However, no clear relationship between compressive strength and the stress state was observed.

The stress-strain behaviour of concrete in compression depends on the stiffness and strength of the coarse fraction of the aggregates and the mortar (the cement and sand fraction). When the concrete is affected by ASR, the stress-strain behaviour changes. Giaccio et al. [2] measured the complete compressive stress-strain behaviour of ASR-affected concrete, and demonstrated increased ductility compared to the non-reactive reference concrete. Mechanical tests of concrete mixes made with various kinds of reactive aggregates were compared at the same expansion level. These tests showed how important the type of reactive aggregate was for the change in mechanical behaviour, which was affected by the mineralogy of the rock, the size of the aggregate and the kinetics of the reaction.

To perform a structural assessment of an ASR-affected concrete structure, tests are needed that can assess the degree of damage and expansion of the concrete. Rivard and Saint-Pierre [11] evaluated non-destructive test methods (ultrasonic pulse velocity, dynamic modulus of elasticity and electrical resistivity), both on laboratory cast specimens and on cores drilled from an hydraulic structure. They showed that non-destructive methods (on cores) were not enable to estimate the mechanical properties of the concrete at various depth of the structure. Even less accurate estimates are therefore expected if these methods are used in field – which is the main purpose of non-destructive testing. The anisotropic nature of ASR damage and the spatial variations of ASR found in concrete structures, make it difficult to assess the damage based physical measures on the surface of the structure. Destructive methods by drilling cores for mechanical testing and petrographic examination are therefore considered to be the most promising tools to assess the current state. Such methods are used and investigated in the present study.

Chrisp et al. [12] proposed to use the stiffness damage test (SDT). The method involves carrying out five loading cycles in compression on cylinders/cores, and then calculating damage parameters from the recorded stresses and strains. Sanchez et al. [13] conducted the SDT on various concrete mixes with different reactive aggregates and different compressive strength. They found that 40% of the compressive strength after 28 days is a sufficient load level to characterize the damage as a function of the expansion level. The modulus of elasticity (E), stiffness damage index (SDI), plastic damage index (PDI), and non-linearity index (NLI) can all be calculated from the SDT, and all these parameters were shown to be correlated with the level of expansion [14]. The SDT has therefore been evaluated as an assessment tool to characterize the damage and the correlated expansion of ASR-affected concrete [13–15]. However, the method has not been used to assess restrained/loaded concrete during the ASR development.

This paper presents the changes in mechanical behaviour of concrete exposed to accelerated ASR conditions and sustained uniaxial compressive stress. The main objective was to investigate the effect of accelerated ASR conditions and uniaxial compressive stress on the evolution of the modulus of elasticity, damage indices obtained from the SDT as described by Sanchez et al. [14], and the evolution of the compressive strength and the compressive stress-strain behaviour of the concrete. In addition, we also investigated the directional dependency (anisotropy) of the mechanical properties created by the uniaxial compressive stress state. The study was carried out to increase knowledge and understanding of ASR-affected concrete and, in particular, its material behaviour, so as to enable accurate structural analysis and assessment. By systematically evaluating the SDT method in restrained and unrestrained directions and by interpreting its results, this paper defines new challenges for the SDT method to become ready for practice.

Section 2 describes the experimental setup for the testing of drilled cores from restrained and free concrete cubes of various ages in terms of days after casting. Section 3 presents the experimental results, including the evolution of the modulus of elasticity, and the strength and damage indicators. Section 4 discusses these results and compares them to the lab and field tests of others. Section 5 provides concise concluding remarks.

2. Materials and methods

2.1. Concrete mix, casting and pre-conditioning

The concrete mix (Table 1) is the same as was used in an ongoing Norwegian ASR experiment [16]. It was intended to represent a concrete typically used in Norwegian bridge structures built in the 1950s and 60s. The aggregates and an almost identical concrete are heavily tested in the EU PARTNER project [17], both in accelerated ASR conditions (Norwegian ASR methods [18] and RILEM AAR-1, −2, −3, −4 [19]) and in field (Fig. 4 and Fig. 10 in [17]). The aggregate composition was also used in a previous Norwegian ASR experimental programme [20]. The concrete mix consists of coarse and fine aggregates in the ratio 3:2 (coarse:fine). The fine aggregate (Årdal 0–4 mm) is a natural sand mainly consisting of granite and gneiss, which is classified as non-reactive according to the Norwegian Concrete Association [18] and RILEM AAR-1, −2 [19]. The coarse aggregate (Ottersbo 4–16 mm) is a reactive crushed cataclasite. The mix design contains 457 kg/m^3 ordinary Portland cement (Norcem Industri, CEM I 42.5R), which has high alkali content (1.24% Na_2O_{eq}) and Blaine specific surface of 575 m^2/kg [21]. The water-to-cement ratio (w/c) is 0.475, which results in an alkali content of 5.6 kg/m^3.

Thirteen large cubes of 230 mm side length and 27 small cubes of 100 mm side length were cast. The concrete moulds were filled and compacted by hand (with a compacting rod) as described in EN 12390-2 [22], and then cured at 20 °C for 24 h under a plastic cover. After demoulding, the concrete cubes were wrapped in soaked jute sacks and plastic sheets, and hardened at 20 °C for 9 days. Eight days after casting, single pairs of expansion measurement points were glued on three surfaces on the large cubes (see Fig. 3), such that expansion could be measured in three spatial directions. The initial lengths between expansion measurement points (approximately 200 mm) were measured the same day.

Table 1
Concrete mix.

Concrete	Quantity [kg/m^3]
Norcem Industri, CEM I 42.5R	457
Årdal sand 0–4 mm	667 (dry weight)
Ottersbo 4–8 mm	172 (dry weight)
Ottersbo 8–11 mm	518 (dry weight)
Ottersbo 11–16 mm	345 (dry weight)
Superplasticizer Sika FB-2	1.4
Water	217
Alkali-content, Na_2O_{eq}	5.6

2.2. Specimen overview and storage conditions

An overview of all the cast specimens is shown in Table 2. Nine days after casting, 9 large cubes were stored in accelerated ASR conditions similar to those described in RILEM AAR-4.1 [19] (60 °C and 100% RH). Five of the cubes (RC60-1,2,3,3b,4) were uniaxially restrained by a low sustained compressive stress, while the other four were free to expand in all directions (FC60-1,2,3,4). Four large cubes remained in storage in the initial hardening conditions (20 °C), all free to expand (FC20-1,2,3,4). Twelve small cubes were stored in accelerated conditions (S60) and 15 under the initial hardening conditions (S20). Considering the short duration of the tests, only limited ASR was expected in the cubes stored at 20 °C, so these were used as reference.

A steel frame inspired by Berra et al. [3] and Kagimoto et al. [4] was used to apply and keep control of a uniaxial stress of 3 MPa on the restrained concrete cubes (RC60), as shown in Fig. 1. The setup consists of two outer steel plates connected by four threaded steel bars. On the day of exposure to accelerated ASR conditions (9 days after casting), a compressive stress of approximately 0.3 MPa was applied to the restrained cubes. The following day (10 days after casting), the bolts were tightened to reach the desired compressive stress of 3 MPa. This two-step procedure was considered necessary to avoid the influence of thermal expansion on the stress state during heating from 20 °C to 60 °C. To sustain an approximately constant compressive stress of 3 MPa, a load cell was placed between the outer plate and a steel plate located on the cube. The load cell was connected to a computer that continuously displayed and recorded the load. During the experiment, the bolts were adjusted to keep an approximately constant stress level within ±0.15 MPa, see Fig. 2. In the beginning, the compressive stress decayed fast due to large concrete creep rates at 60 °C, which made it difficult to maintain the stress. After the second load adjustment, 5 days after loading, the reduction in stress due to creep was minor. A small increase in stress due to ASR expansion can be noticed from the figure.

The stress was always applied perpendicular to the casting direction. A layer of Teflon was added between the cube and the steel plates to minimize the friction between the steel plates and the concrete when the concrete expands due to ASR. Steel plates were also placed on the top and bottom surfaces of the cubes that were free to expand (FC60) in order to achieve similar boundary conditions with respect to moisture transport, for both restrained and free cubes.

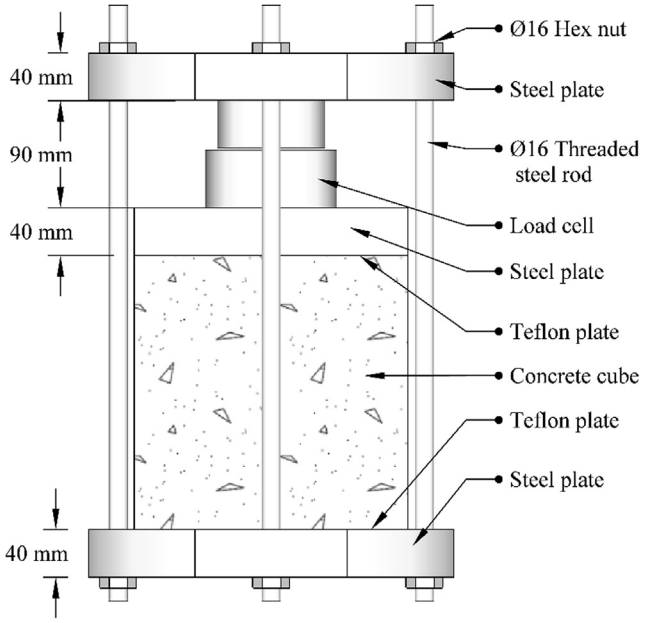

Fig. 1. A sketch of the steel frame used to restrain the concrete cubes.

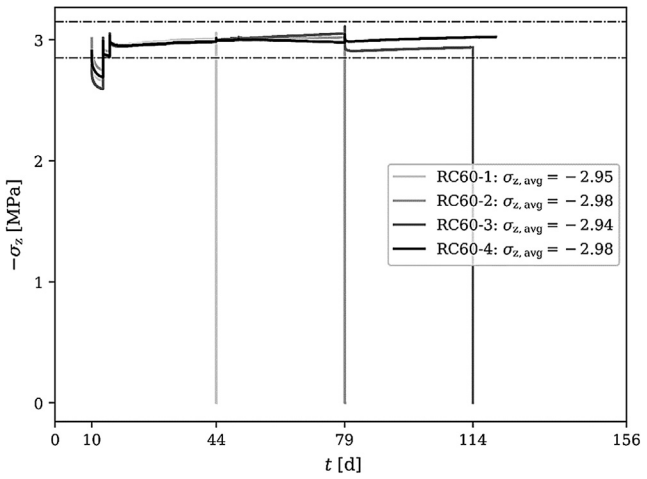

Fig. 2. Measured stress on restrained cubes (RC60). Dashed lines indicate 3 MPa ± 0.15 MPa. The average stress (from loading to unloading) for each cube is given in the legend.

2.3. Expansion measurement and preparation for mechanical testing

The cubes from accelerated ASR conditions were prepared for expansion measurement and further mechanical testing at 44, 79, 114 and 156 days after casting. First, the compressive stress was removed on the restrained specimen (RC60). Then, both the restrained (RC60) and free (FC60) cube were cooled in a two step-procedure: first in a room at 38 °C for one day, and then three days in a room at 20 °C. The cubes were kept in their buckets during the cooling procedure to limit drying. After cooling, the distance between each pair of measurement points on the cubes' surfaces were measured with a distance gauge (extensometer) with micrometre accuracy. The expansion/strain was obtained as the ratio of the relative displacements to the initial distance that was measured before the accelerated conditions were applied (8 days after casting).

From the restrained cubes, two cores were drilled parallel and two perpendicular to the restrained direction (see Fig. 3), while from the free cubes, two cores were drilled in only one direction

Table 2
Specimen overview and storing conditions.

Cube tag	Amount	Size	Temperature[°C]	Relative Humidity	Restrained/Free
RC60	5	$(230\ mm)^3$	60	~100%	Restrained
FC60	4	$(230\ mm)^3$	60	~100%	Free
FC20	4	$(230\ mm)^3$	20	95–100%	Free
S20	15	$(100\ mm)^3$	20	95–100%	Free
S60	12	$(100\ mm)^3$	60	~100%	Free

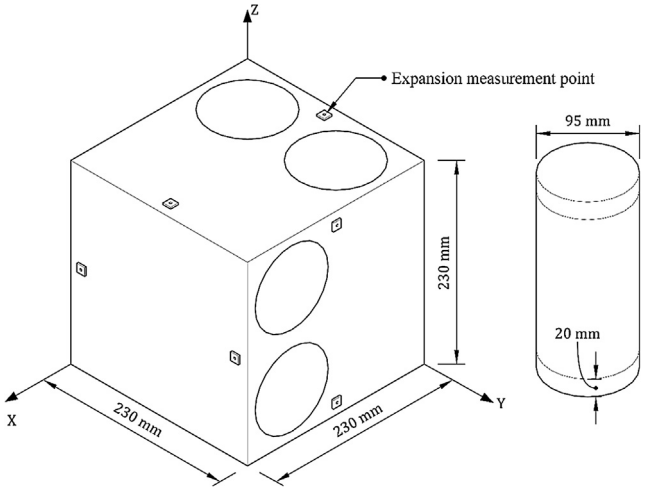

Fig. 3. Two cores were drilled from the restrained cubes in two directions (Y and Z). The cubes were cast along the X-axis; the Z-axis is the restrained direction.

(because of isotropic conditions). All of the cores were drilled perpendicular to the casting direction (X). The coring was performed with a bit of 100 mm in outer diameter, resulting in cores of approximately 95 mm in diameter. Water was supplied during the process to avoid excess of heat. To ensure even stress distribution during mechanical compressive testing, the end surfaces were sawn and ground perpendicular to the longitudinal axis of the cores.

After drilling and sawing, the cores were stored on a wet towel under a plastic sheet to avoid drying. The stiffness damage test, compressive strength test and complete compressive stress-strain test were all conducted the day after drilling.

2.4. Methods for mechanical testing and assessment

Table 3 gives an overview of the mechanical tests that were conducted on the cores drilled from the large concrete cubes. For each core, the stiffness damage test (SDT) was first conducted. Then, the core was further tested by either the compressive strength test or the complete compressive stress-strain test. The RC60-i-Zj cores were drilled in the restrained direction. The RC60-i-Yj were drilled in the unrestrained direction that is not the cast direction.

We used the SDT as recommended by Sanchez et al. [13]. Their test includes five load cycles in compression, where the applied stress and the corresponding longitudinal strain are recorded during the test. We also adopted their recommendation of a load level equal to 40% of compressive strength at 28 days after casting. In our study, the compressive cylinder strength after 28 days was estimated based on the compressive cylinder strength of the reference cube FC20-1 50 days after casting and assuming the evolution of strength described in EN1992-1-1 [23]. The 50-day cylinder strength used was the average of two cores, see Table A.1 in Appendix. This resulted in a maximum stress of 16.2 MPa in each load cycle. The samples were compressed in a load controlled manner at a load rate of 0.10 MPa/s until the desired stress of 16.2 MPa was reached, and then the load was reduced by 0.10 MPa/s until 1.5 MPa was reached. The maximum and minimum stress levels were maintained for less than four seconds. The lower limit of 1.5 MPa was used to prevent the load frame from losing connection with the sample. The SDT was conducted using a "Form + Test Alpha 4/B-62" compressive load frame, and the start, stop, increase and decrease in load during the load cycles were manually controlled.

The longitudinal strain was obtained by a measuring device that was attached to the core during the SDT. This measured the relative displacement in the longitudinal direction between two points at three equidistant locations (separated by an angle of 120°) around the circumference of the core, see Fig. 4. The initial (or measurement) distance between the points is approximately 100 mm. The strain was calculated as the average of the three relative displacements divided by the measurement distance equal to 100 mm.

The modulus of elasticity (E_{SDT}), and the three parameters Stiffness Damage Index (*SDI*), Plastic Deformation Index (*PDI*), and Non-linearity Index (*NLI*) were calculated from the measured stress-strain relationships. The parameters are as follows:

- *SDI*: The ratio of dissipated energy to the total energy implemented in the system, given by Eq. (1). It is the sum of the dissipated energy (*SI*) for each load cycle divided by the sum of total energy (*SI* + *SII*) for each load cycle. An illustration of *SI* and *SII* (for the first load cycle) is shown in Fig. 5.

$$SDI = \frac{\sum_{i=1}^{5} SI_i}{\sum_{i=1}^{5} (SI_i + SII_i)} \quad (1)$$

- *PDI*: The plastic deformation accumulated during the SDT (*DI*) divided by the total deformation measured at maximum load in the last cycle (*DII*), see Fig. 5.
- *NLI*: The secant stiffness at half of the maximum load, divided by the secant stiffness at maximum load in the first load cycle. The secant lines are shown in Fig. 5.
- E_{SDT}: The average secant stiffness of the unloading curves for the second, third and fourth load cycle.

The compressive stress-strain test was conducted on 12 selected cylinders after the SDT, see Table 3. The test was conducted with a 5000 kN compressive frame from Losenhausen in accordance with the procedure in Norwegian Standard 3473 Appendix A, pkt. A.11.3.1. The test was deformation-controlled with a constant strain rate of approximately 0.03%/min. Three linear variable differential transformers measured the displacements between steel plates at each end of the core. The measured displacements therefore include those of the boundaries of the specimen and those of the concrete. From the stress-strain relationships, the modulus of elasticity was calculated as the secant stiffness at 40% of the compressive strength. Fracture energy in compression was calculated as defined by Nakamura and Higai [24]; see Fig. 6 for an illustration of the definition. One core in each direction of the ASR-affected and restrained cubes (RC60) was tested in each of the four test rounds. The stress-strain behaviour of cores from reference cubes (FC20) was also measured in the first two test rounds. The compressive strength test (EN 12390-3 [25]) was conducted on the cylinders that were not tested for compressive stress-strain behaviour. The compressive strength test (EN 12390-3 [25]) was also conducted on small cubes (100 × 100 × 100 mm) at 30, 48, 83, 118 and 160 days after casting. Table 4 gives an overview of the quantities that were calculated from the mechanical tests.

2.5. Method for mapping of micro crack orientation

A fifth concrete cube, restrained and stored in accelerated ASR conditions, was used for petrographic examination (RC60-3b). This cube followed the same storage conditions as cube RC60-3 up to the day of expansion measurement (118 days after casting). After expansion measurement, this cube was wrapped in cling film

Table 3
Overview of the mechanical tests conducted on the cores drilled from the cubes.

Cube	Drilled core	Age at testing in days after casting	SDT	Compressive strength test	Compressive stress-strain test
FC20-1	FC20-1-Y1	50	X		X
	FC20-1-Y2	50	X	X	
FC20-2	FC20-2-Z1	85	X		X
	FC20-2-Z2	85	X	X	
FC20-3	FC20-3-Z1	120	X	X	
	FC20-3-Z2	120	X	X	
FC20-4	FC20-4-Z1	162	X	X	
	FC20-4-Z2	162	X	X	
FC60-1	FC60-1-Y1	50	X		X
	FC60-1-Y2	50	X	X	
FC60-2	FC60-2-Z1	85	X		X
	FC60-2-Z2	85	X	X	
FC60-3	FC60-3-Z1	120	X	X	
	FC60-3-Z2	120	X	X	
FC60-4	FC60-4-Z1	162	X	X	
	FC60-4-Z2	162	X	X	
RC60-1	RC60-1-Y1	50	X		X
	RC60-1-Y2	50	X	X	
	RC60-1-Z1	50	X		X
	RC60-1-Z2	50	X	X	
RC60-2	RC60-2-Y1	85	X		X
	RC60-2-Y2	85	X	X	
	RC60-2-Z1	85	X		X
	RC60-2-Z2	85	X	X	
RC60-3	RC60-3-Y1	120	X		X
	RC60-3-Y2	120	X	X	
	RC60-3-Z1	120	X		X
	RC60-3-Z2	120	X	X	
RC60-4	RC60-4-Y1	162	X		X
	RC60-4-Y2	162	X	X	
	RC60-4-Z1	162	X		X
	RC60-4-Z2	162	X	X	

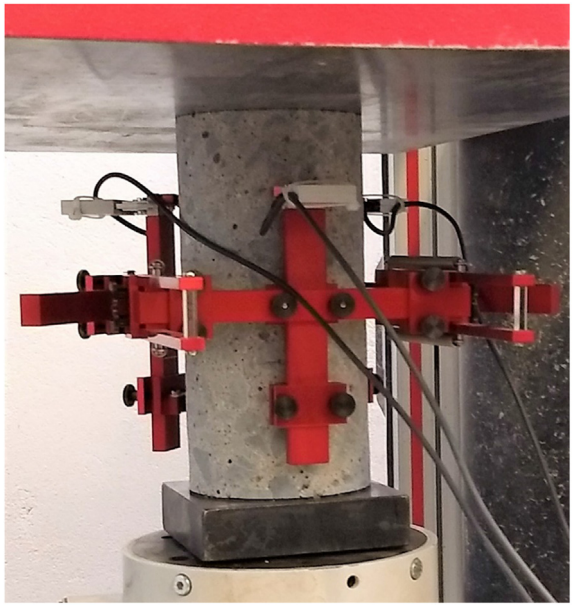

Fig. 4. Strain measurement during the stiffness damage test.

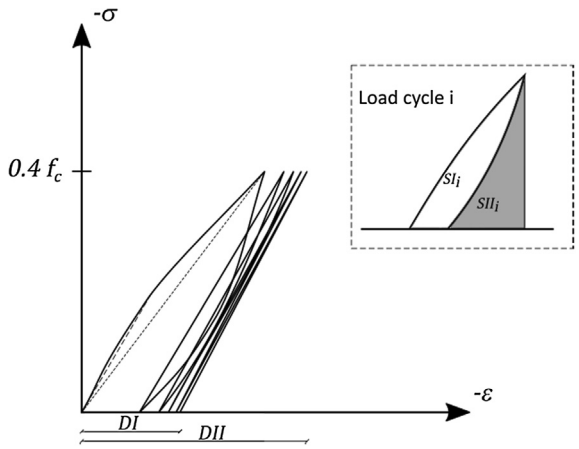

Fig. 5. Definition of the values used to calculate the indices from the stiffness damage test.

and stored for six months at 20 °C. Negligible expansion was observed over this storage period. Then, a core was drilled in the restrained direction (Z), which afterwards was sawn along the same axis to obtain a plane section. The section was impregnated with fluorescent epoxy for ultraviolet (UV) photography. This photographic method gives images with high contrast between cracks and their surroundings (suitable for image processing). Andreassen et al. [26] used image analysis to quantify the orientation of micro cracks in concrete affected by ASR. They used a gradient method (by convolution of the greyscale image with a 3 × 3 Prewitt kernel) to detect edges (cracks) and their orientation. Pixels with gradient magnitude above a threshold value were considered as crack pixels. Crack pixel gradient orientations were rounded to the nearest integer angle in 0–180, and crack orientation distribution was obtained by counting crack pixels belonging to each integer angle and dividing to the total amount of crack pixels – length of the cracks was therefore not considered.

In this study, we also used image analysis to quantify the main micro crack direction, but we used a different approach to take into account the length of cracks. The procedure consists of the following steps, where the first two steps are similar to Andreassen et al. [26]:

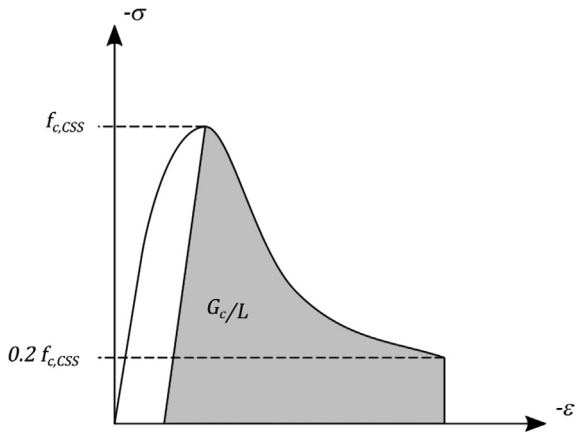

Fig. 6. Illustrative definition of fracture energy in compression as defined by Nakamura and Higai [24]. G_c is the fracture energy and L is the length of the core.

1. **Grey scale conversion.** The original image's green level was mapped to grey scale, i.e. a number for each pixel between 0 (black) and 255 (white).
2. **Edge (crack) detection.** The greyscale image was convolved with two 3 × 3 Prewitt kernels, to obtain the gradient in row and column direction. The gradient magnitude is calculated similar to Andreassen et al. [26].
3. **Binary image conversion.** All pixels with magnitude greater than the threshold are set to 1 (white), else set to 0 (black).
4. **Noise reduction.** All components, i.e. all isolated white islands on black background, were identified by a connected component labelling algorithm. Small components containing less than a specific amount of pixels were considered as noise and therefore removed.
5. **Ellipse fitting and removal of circular components.** An elliptical fit to all remaining components was conducted. The circularity (roundness) of the components was evaluated by the aspect ratio (width/length) of the ellipses, and all components with aspect ratio greater than a threshold was removed. By this procedure, we removed air pockets that was filled by the fluorescent epoxy, which showed up as almost circular components.
6. **Calculation of crack orientation distribution.** The remaining components were considered as cracks, and the ellipses length and principal axis orientation were used to map the micro crack orientation.

The applied threshold values will be specified when presenting the results in Section 3.5.

3. Results

3.1. Expansion

The expansion of the large cubes in the X, Y and Z directions against days after casting are shown in Fig. 7 a–c, where the X-axis represents the casting direction and the Z-axis corresponds to the loaded direction for the restrained cubes (RC60). The volumetric expansion of the cubes is shown in Fig. 7 d. The expansions of each cube was only measured at the time of testing; the curves in Fig. 7 were obtained by combining the expansion measurements from different cubes at different times.

3.2. Stiffness damage test (SDT)

Fig. 8 shows a representative selection of the stress-strain curves obtained during the stiffness damage test. The plots are in order of increasing expansion from 0.002% in a) to 0.257% in d). The figure shows an increase in plastic deformation and hysteresis area with increasing expansion. From each stress-strain relationship, the modulus of elasticity and SDT-indices (SDI, PDI and NLI) were calculated, and the results are presented in the following sections.

3.2.1. Modulus of elasticity

Fig. 9 shows the development of the modulus of elasticity with respect to time, measured in days after casting. The figure shows a reduction in the modulus of elasticity for all ASR-affected samples, while the modulus of elasticity of the reference samples is approximately constant throughout the experiment. Less reduction in the modulus of elasticity is found in the restrained direction (z-axis).

In Fig. 10, the relative modulus of elasticity of the ASR-affected samples is plotted against the level of expansion of the cube in the coring direction. The values are relative to the average modulus of elasticity of the reference cubes. Also included in the plot is a model function (Wen [27]), which was fitted to the data using the least squares method. This function can be derived based on a simple series model, in which the ASR-affected concrete is composed of healthy concrete with a modulus of elasticity equal to that of the reference concrete, and damaged concrete with a reduced modulus of elasticity [27]. The grey dotted lines indicate the upper and lower bounds from a study by Sanchez et al. [15] on various concrete mixes.

3.2.2. SDT indices

In Figs. 11 and 12, the stiffness damage index (SDI) and the plastic damage index (PDI) are plotted against expansion in the drilled direction. Again, model functions were fitted to the data using the least squares method.

In Fig. 13, the non-linearity index (NLI) is plotted against expansion together with a linear trend line (with an R^2 of 0.83). An overall low NLI is found for cylinders extracted in the restrained direction of the ASR-affected cubes.

3.3. Compressive strength

The compressive cube strength results are presented in Fig. 14. Compared to the strength of the reference samples at 30 days after casting, the test results at 48 days after casting show a significant increase in strength for both the cubes stored in accelerated ASR conditions and the reference cubes stored at 20 °C. However, in the last three tests, lower strength was found for the samples exposed to accelerated ASR conditions than for the references. The strength of the reference samples continued to increase over

Table 4
Measured and calculated quantities from the mechanical tests.

SDT	Compressive strength test	Compressive stress-strain test
E_{SDT}, modulus of elasticity *SDI*, stiffness damage index *PDI*, plastic damage index *NLI*, non-linear index	f_c, compressive strength	E_{CSS}, modulus of elasticity $f_{c,CSS}$, compressive strength G_c, fracture energy in compression

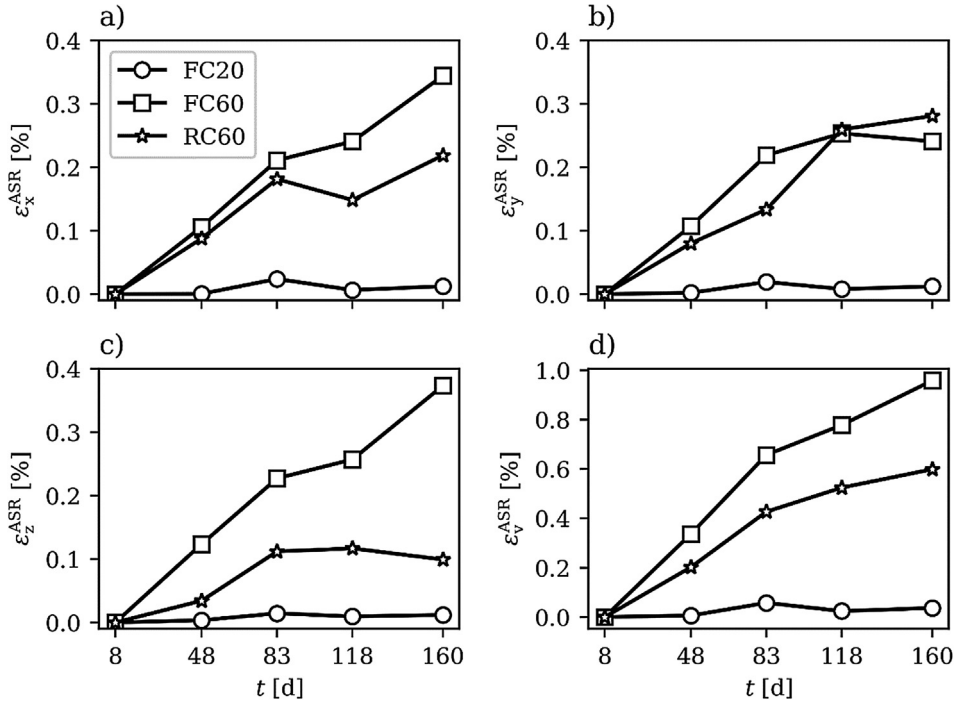

Fig. 7. a) expansion in X-direction, b) expansion in Y-direction, c) expansion in Z-direction, and d) volumetric expansion.

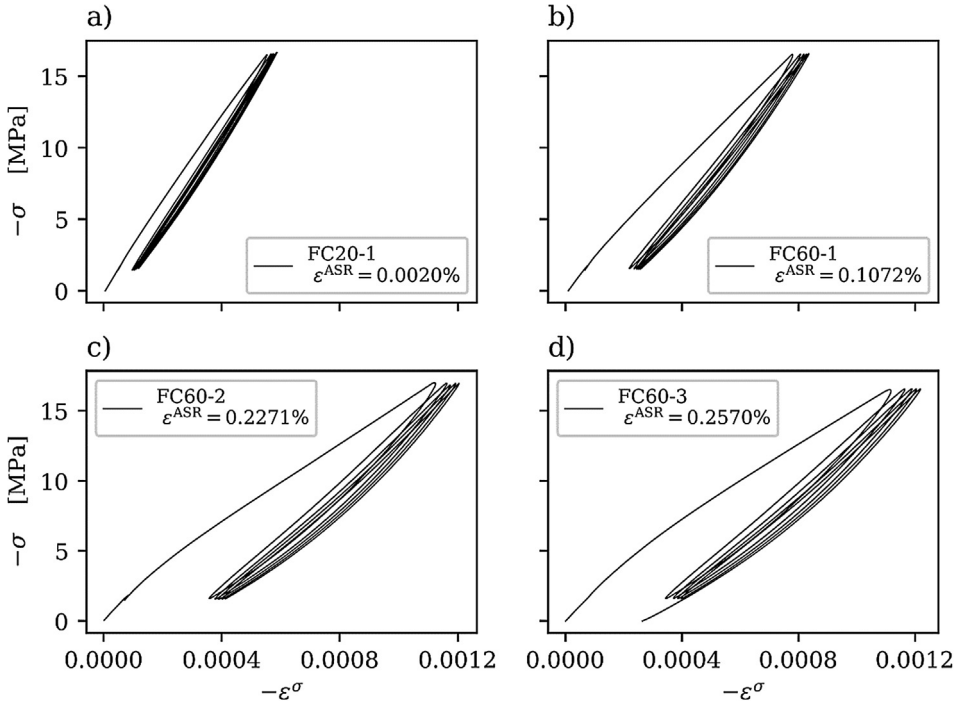

Fig. 8. A selection of stress-strain curves from the SDT sorted, from low to high levels of axial expansion due to ASR.

the testing period, while the ASR-affected samples displayed almost constant strength.

The evolution of the compressive cylinder strength is presented in Fig. 15. At 50 days, compressive cylinder strength is greater for all ASR-affected cubes than for the reference, but while the strength of the reference increases with age, a reduction is observed for the freely expanding ASR-affected cubes. The compressive strength in the restrained direction of RC60 is almost constant, while a slight decrease is found in the unrestrained direction.

In Fig. 16, the relative cylinder compressive strength is plotted against the degree of expansion. The linear trend line shows a small reduction in compressive strength with increasing expansion. The coefficient of determination is as low as $R^2 = 0.027$.

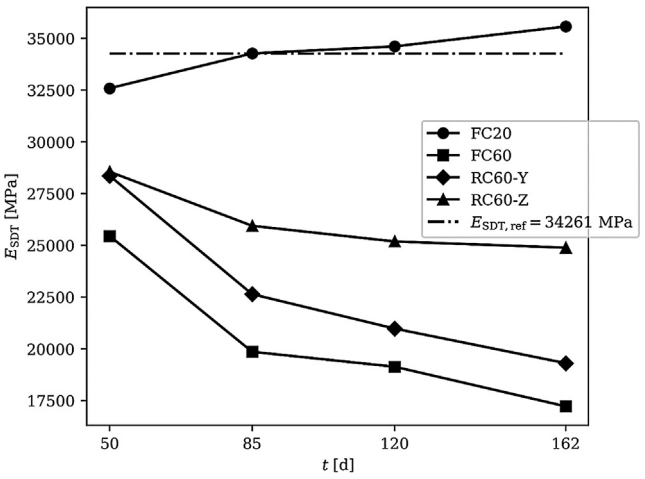

Fig. 9. Modulus of elasticity plotted against time in days after casting.

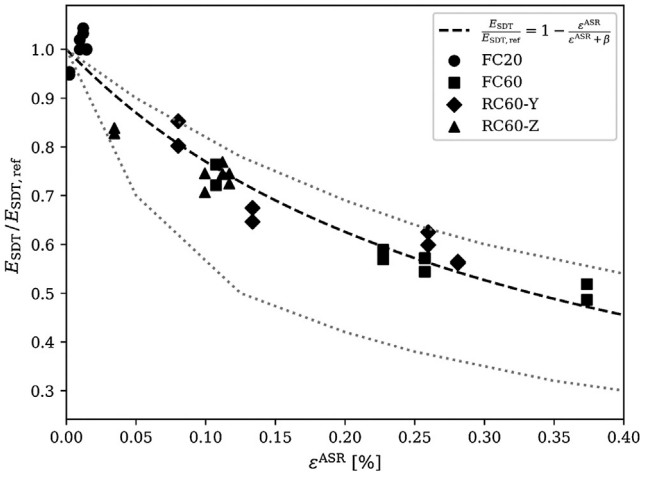

Fig. 10. Development of the relative modulus of elasticity with respect to ASR expansion. The coefficient in the regression function is $\beta = 0.0033$ and the coefficient of determination is $R^2 = 0.94$.

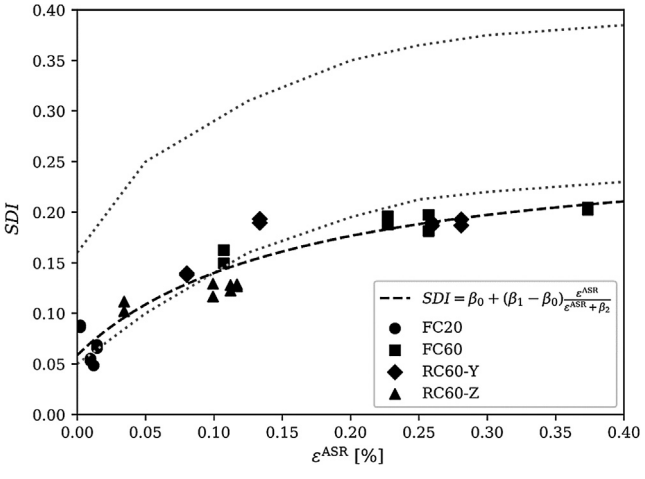

Fig. 11. SDI against expansion. A regression function is also included with$\beta_0 = 0.059$, $\beta_1 = 0.273$ and $\beta_2 = 0.00164$. The coefficient of determination is $R^2 = 0.88$.

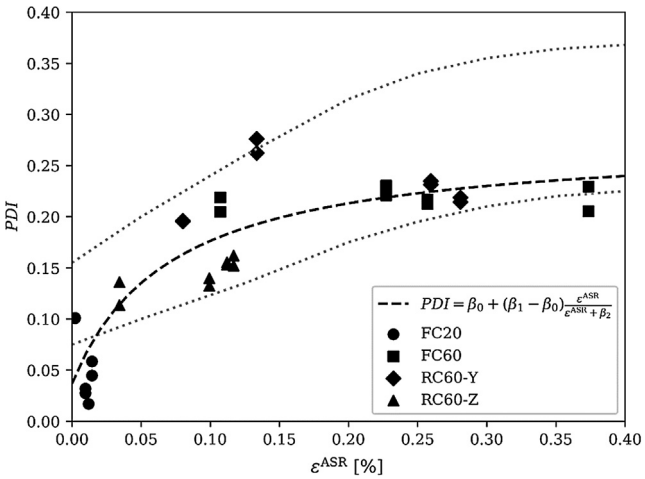

Fig. 12. PDI against expansion with a trend curve. $\beta_0 = 0.037$, $\beta_1 = 0.276$ and $\beta_2 = 0.00071$.$R^2 = 0.76$.

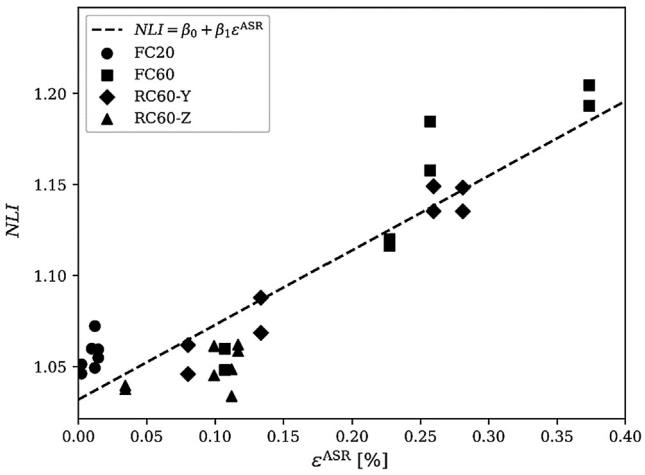

Fig. 13. NLI plotted against expansion with a linear trend curve. $\beta_0 = 1.032$, $\beta_1 = 41.0$.$R^2 = 0.83$.

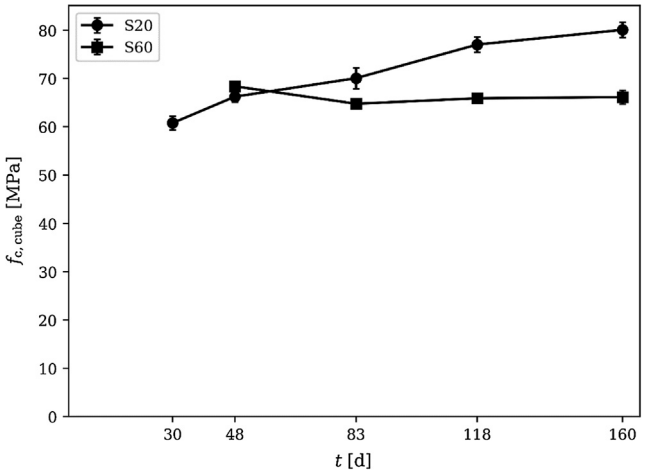

Fig. 14. Compressive cube strength against days after casting. The values are the average strength of three cubes, and the error bars show the standard deviation.

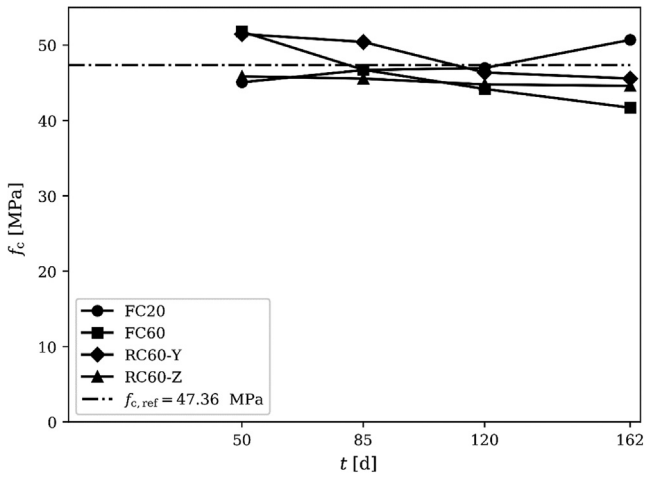

Fig. 15. Cylinder compressive strength against days after casting.

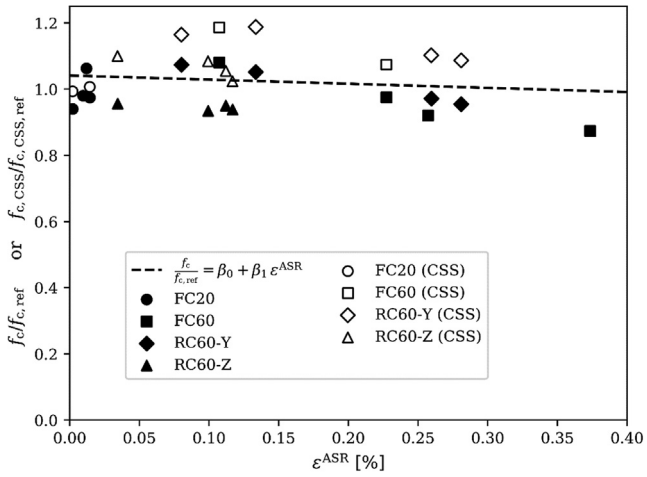

Fig. 16. Relative cylinder compressive strength against expansion. $\beta_0 = 1.047$ and $\beta_1 = -12.7$.$R^2 = 0.027$.

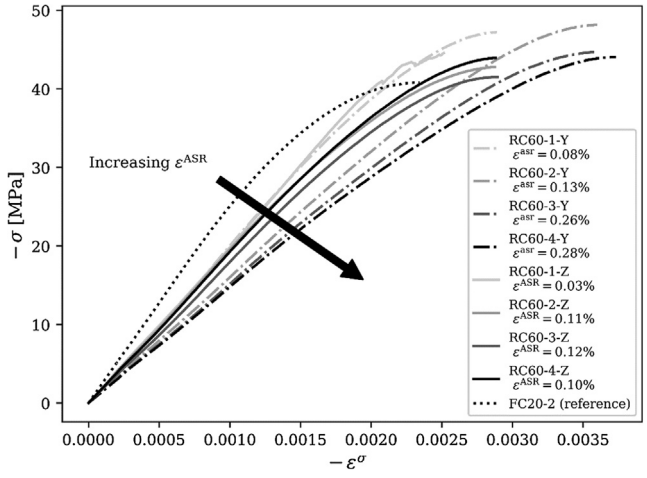

Fig. 17. Stress-strain curves in compression of ASR-affected and restrained specimens (RC60). Dashed lines indicate the cylinders that are drilled in Y-direction (free direction) and solid lines represent the cylinders that are drilled in Z-direction (restrained direction).

3.4. Compressive stress-strain behaviour

Fig. 17 shows the stress-strain curves in compression up to the peak stress ($f_{c,CSS}$) of the restrained and ASR-affected cubes (RC60). The curves are labelled with the corresponding expansion due to ASR. The figure shows that the stiffness decreases with increasing ASR expansion. The ductility in terms of strain at peak stress increases with increasing ASR expansion, see Fig. 18.

The relative modulus of elasticity and the relative fracture energy in compression are plotted in Figs. 19 and 20 against the longitudinal and maximum transversal ASR strain, respectively. The values are relative to the average value of the reference cubes (FC20).

3.5. Expansion and micro crack orientation of restrained cube RC60-3b

The expansion of the cube RC60-3b at 118 days after casting was 0.24%, 0.26% and 0.15% in the X, Y and Z direction. Fig. 21 shows the intermediate and final results of the petrographic examination of a core drilled in the strained direction (Z) of RC60-3b. Fig. 21 a) shows the resulting image obtained by UV photography. Fig. 21 b) shows the binary image, resulting after step 3, see Section 2.5, where a gradient threshold of 50 was used. Fig. 21 c) shows the final processed image, i.e. the resulting image after removing small components containing less than 100 pixels (step 4) and almost circular components with aspect ratio (length/width) less than 0.4 w (step 5). The fitted ellipses are also included (shown in red).

The ellipses length and principal axis orientation were used to evaluate the crack orientation distribution. Fig. 22 shows the distribution of crack orientation in intervals of 20°. The angle was measured counter clockwise from the horizontal axis. One can see that most of the cracks are aligned with the vertical direction (90°), which coincides with the restrained direction (Z).

4. Discussion

4.1. Expansion and micro cracking

The expansion measurement of each cube was taken at the time of testing, and then the data points were combined to obtain the graph in Fig. 7. This means the development of the expansion with respect to time is only valid if all the cubes expand equally, which is uncertain. Furthermore, the expansion in a given direction is

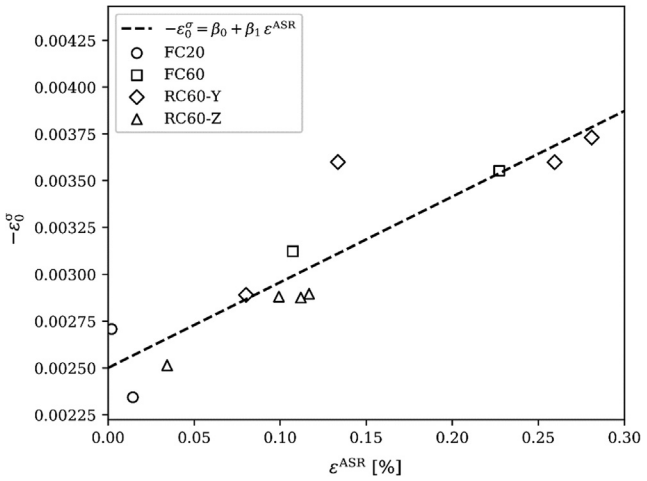

Fig. 18. Peak compressive strain against ASR expansion. The coefficients in the regression function are $\beta_0 = 0.0025$ and $\beta_1 = 0.45$. $R^2 = 0.82$.

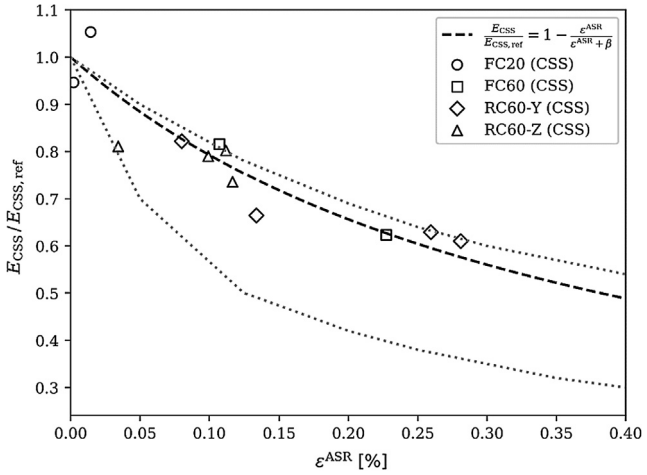

Fig. 19. Development of relative modulus of elasticity, obtained from the compressive stress strain test, against ASR expansion. $E_{CSS,ref} = 24302$MPa. The coefficient in the regression function is $\beta = 0.0038$, and the coefficient of determination is $R^2 = 0.83$.

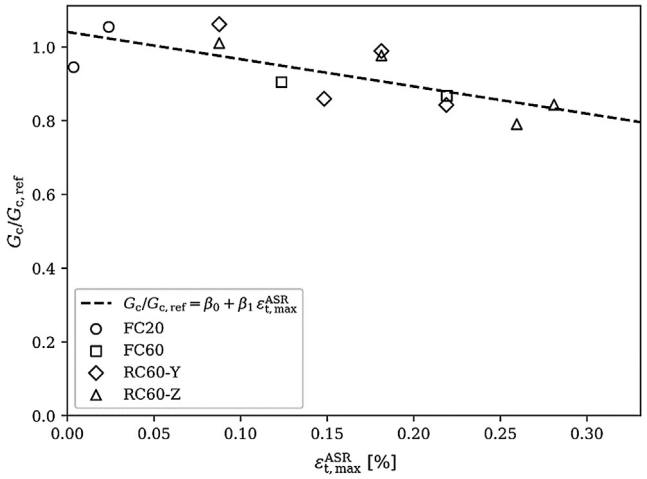

Fig. 20. Relative fracture energy in compression against the maximum transversal expansion due to ASR. $G_{c,ref} = 36.5$N/mm. $\beta_0 = 1.04$ and $\beta_1 = -74$. $R^2 = 0.53$.

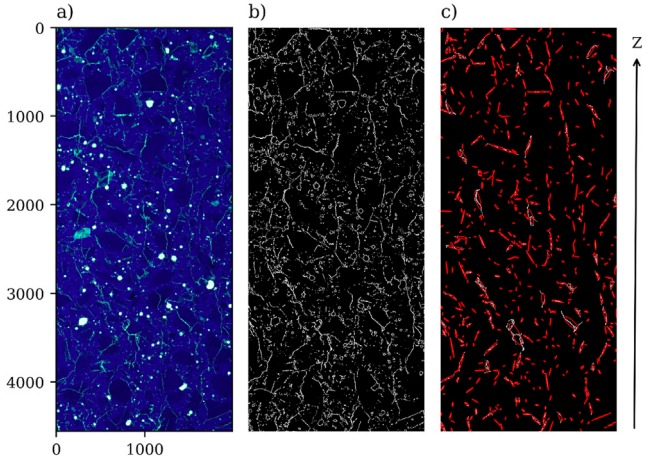

Fig. 21. Petrographic examination results of RC60-3b with a) cropped original image, b) binary image, and c) final processed image.

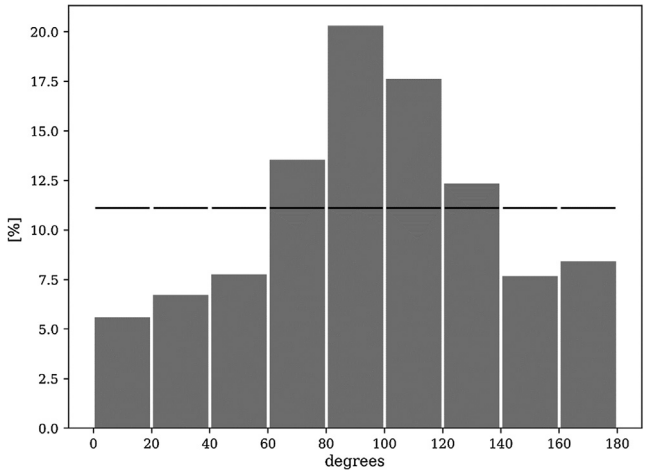

Fig. 22. Crack orientation distribution. Angles are measured counter clockwise from the horizontal axis. Black lines are the bar height for a uniform distribution.

obtained from one pair of measurement points attached to the cube surface. This measurement will therefore only represent the average expansion in the case of almost homogeneous strains, so if there is significant spatial variation, the validity of the expansion measurement becomes questionable. A better approximation of the average expansion could have been obtained by using several pairs of measurement points in each direction, but this was a matter of resources, and in the following we had to assume that the strains were sufficiently homogeneous throughout the specimen for us to obtain the expansion of the cores at the time of testing. The SDT damage indices, the compressive strength, and the relative modulus of elasticity were all plotted against these expansions.

Four expansion behaviours can be found in the literature if at least one direction is free of stress: 1) total transfer of expansion to the stress-free directions, i.e. volumetric expansion is preserved [1,5,10], 2) partial transfer [3,4,7], 3) no or negligible transfer to the stress-free directions [6,28], and 4) the expansion in the stress-free directions is reduced [29,30]. In the present work, lower volumetric expansion in restrained cubes than in free cubes was observed. Furthermore, no expansion transfer to the stress-free directions is observed, which indicates that the concrete mix (studied in this work) belongs to either expansion behaviour type 3 or 4. However, as the expansions were measured after unloading (and the cubes were cooled to 20 °C), in contrast to the mentioned studies from the literature, the results might not be comparable. In addition, the low number of test specimens in our study makes it difficult to place the concrete mix in one of the four categories.

It should be noted that the differences in expansion behaviour can be attributed to other differences than the concrete mix. The influence of specimen size to the size of reactive aggregates was experimentally investigated on mortar prisms by Gao et al. [31], and the results were explained by fracture mechanics concepts; the specimen to aggregate size must be sufficiently high to reduce this scale effect. The influence of the casting direction, as described by Smaoui et al. [32], is explained by two reasons: 1) porous and weak zones under the aggregates due to trapped water, resulting in lower resistance along the casting plane to the expansive pressure developed by ASR, and 2) preferred orientation of elongated aggregates along the casting plane, creating higher areas of expanding aggregates along this plane. Both phenomena are influenced by the compaction/consolidation method, where using a vibrating table or vibrating needle give greater intrinsic anisotropy of the concrete than using a compacting rod [32] – which has been used in this investigation. Lateral restraint on the loaded boundary of the specimens undergoing ASR might cause shear stresses, and

therefore a triaxial stress state even in "uniaxial sustained loading". This effect is similar to what is observed for compressive testing of concrete (due to lateral expansion under compressive stress), which gives rise to a size effect. This effect is minimized in this work by adding Teflon in between concrete and steel.

The results on the expansion and micro crack orientations of the restrained cube RC60-3b, in Section 3.5, show that the main cracking direction is parallel to the restrained direction.

4.2. SDT-parameters

4.2.1. Modulus of elasticity

As in previous studies [2,8,15,27,33–35], the modulus of elasticity decreased with increasing expansion due to ASR, as shown in Fig. 10. Sanchez et al. [15] studied the evolution of the relative modulus of elasticity for 20 different concrete mixes composed of 13 different aggregates. Figs. 10 and 23 show the upper and lower bounds of the relative modulus of elasticity (indicated by dotted lines) found by Sanchez et al. for these concrete mixes. The results in the current study are close to the upper bound. The values for the relative modulus of elasticity obtained from both the SDT and the complete compressive stress-strain (CSS) test are included in Fig. 23, i.e. the values from Fig. 10 and 19. The modulus of elasticity obtained by the two test methods differs a lot, but the relative values are very similar (we attribute the difference in stiffness to the methods used for deformation measurement). It should be noted that Sanchez et al. used the modulus of elasticity (along with SDI, PDI and NLI) of the reference concrete at an equivalent age in the calculation of relative values, in accordance with the maturity concept.

The model function (Wen [27]) fitted to the results in the current study gives $\beta = 0.0035$, while $\beta = 0.002$ was obtained on the concrete he tested [27], see Fig. 23. The evolution of the relative modulus of elasticity differs a lot between concrete mixes, but Wen's model function [27] is applicable to a variety of mixes by changing the coefficient β. Fig. 23 also shows the S-shaped curve of Esposito et al. [35] fitted on data available in the literature on the (static) modulus of elasticity of ASR-affected concrete under free-expansion. Esposito et al. used the modulus of elasticity at 0.05% expansion as the reference value, which partly explains why their trend curve shows less deterioration. Significant lower stiffness is observed for ASR-affected concrete at this level of expansion, which gives higher calculated relative values.

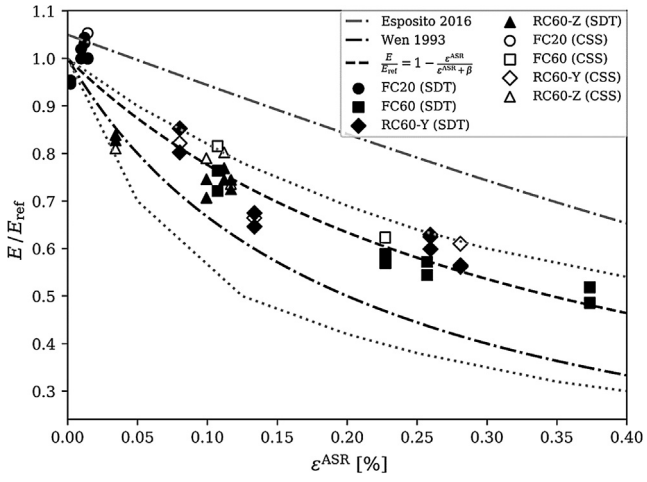

Fig. 23. Relative modulus of elasticity against expansion. Upper and lower bounds from the experimental work of Sanchez et al. [15] are indicated with grey dotted lines. The coefficient in the model function is $\beta = 0.00346$ and the coefficient of determination is $R^2 = 0.916$.

Similarly to the expansion behaviour, an anisotropic stiffness reduction is observed in the present work for the restrained specimens, where greater reduction in modulus of elasticity is found in the free directions (X and Y) than in the direction with sustained loading (Z). The reduction of modulus of elasticity in a particular direction is explained by one causal variable, i.e. the expansion in the same direction, see Fig. 10. Furthermore, the evolution of modulus of elasticity vs. ASR expansion resembles the function coming from the one-dimensional series model of Wen [27]. These are interesting observations from a constitutive modelling point of view. Wen developed a constitutive model in which he included this stiffness reduction due to ASR; however, the stiffness was isotropically reduced, where the maximum principal ASR strain was used as the argument in the model function. The anisotropic stiffness reduction was accounted for in the constitutive model of Capra and Sellier [36] (later developed in [37,38]). In these models [36–38], stiffness is reduced in an orthotropic damage framework by employing an independent evolution of modulus of elasticity vs. ASR expansion in three orthogonal directions. The notion that the three orthogonal directions can be treated individually is in accordance to what is observed in the present investigation. It should be noted that it can be shown that the evolution of modulus of elasticity vs. ASR expansion used in [36–38] is equivalent to the model function developed by Wen [27].

4.2.2. SDI, PDI and NLI

In Figs. 11 and 12, the SDI and PDI values are plotted together with the upper and lower bounds (dotted lines) from the experimental programme by Sanchez et al. [15]. The SDI values are closer to the lower bound, i.e. small damage for high expansions, which is consistent with the evolution of relative modulus of elasticity close to the upper bound in Fig. 23. The PDI values are more scattered than the SDI values, with some values beyond the upper bound.

The main contribution to the SDI is the energy dissipation related to the first load cycle. We assume that most of the dissipation is due to the formation of new micro cracks with crack planes parallel to the loaded direction. This can be justified by the experiments of Giaccio et al. [2], where they measured the lateral strain during compressive stress strain test, and showed an increase in the lateral/axial strain ratio for ASR-affected concrete, even for stresses below 40% of compressive strength. Furthermore, we believe the energy dissipation during the first cycle depends on the degree and orientation of existing micro cracks due to ASR.

We can compare two cores that have the same axial expansion, but different lateral expansion due to ASR. During the first load cycle of the SDT, it is reasonable that more splitting micro cracks will be formed for the specimen with the least amount of existing cracking along the core, i.e. the specimen with the least lateral expansion. This means that the energy dissipation during the first load cycle, and consequently SDI, will be different for the two cores with the same axial expansion due to ASR. This is apparent in Fig. 11, where the cores drilled in the direction of sustained load have a lower SDI than cores in the free direction for the same axial expansion value. In the early development of the SDT for application on ASR-affected concrete (Chrisp et al. [12]), it was recognized that the degree of damage measured in terms of modulus of elasticity and dissipation of energy was a combination of pre-existing ASR damage and additional damage caused by the first load cycle. The maximum load of the SDT was therefore set to a low level (15% of compressive strength) to limit the load-induced damage of the first load cycle. Moreover, the data of the first cycle was discounted. In more recent recommendations on SDT [13,14], used in this research, 40% of the compressive strength and inclusion of the energy dissipation of the first load cycle are recommended. However, this is in contrast to the above-mentioned test philosophy by Chrisp et al. [12], which might be more

important to maintain when testing anisotropically ASR-damaged concrete.

The NLI represents the concavity (or convexity) of the ascending stress-strain curve for the first load cycle. Fig. 13 shows that the NLI is above one (i.e. concave shape) for all cores. Furthermore, the NLI increases with expansion due to ASR. If we instead consider the NLI of subsequent load cycles by the average NLI for load cycles 2–5, as originally proposed by Chrisp et al. [12], NLI is below one (i.e. convex shape) and decreases with expansion, see Fig. 24 for a comparison. The concave shape of the first cycle, and the convex shape of the subsequent cycles, confirm that additional damage is primarily induced in the first cycle. Moreover, the convex shape, i.e. increasing tangential stiffness with loading, indicates progressive closing of micro cracks. The latter four cycles are therefore characterised by progressive closing and opening of micro cavities (due to both ASR and additional damage from first cycle) when loading and unloading, respectively.

4.3. Compressive strength

Unlike the modulus of elasticity and the SDT-indices SDI, PDI and NLI, no correlation is apparent between compressive strength and expansion level, as can be seen in Fig. 16. However, the results are still worth discussing due to the influence of several important aspects such as temperature history, moisture conditions, and cracking, as well as the expansion itself.

The higher compressive strengths measured at the first two testing times (50 and 85 days) for the concrete exposed to the accelerated ASR conditions are probably due to the favourable effect of the increased temperature and the extremely humid conditions. It is well known from concrete technology that higher curing temperatures can have a negative impact on compressive strength after 28-days, in particular if ordinary Portland cement is being used (e.g. see Balendran and Martin-Buades [39]), but this is usually explained by a coarser microstructure caused by rapid hydration during the first hours after water addition. In the present investigation, however, the temperature was increased from 20 to 60 °C when the specimens were 9 days old, and a negative effect was therefore not expected. On the contrary, we expected the main net effect of the increased temperature to be accelerated strength development in accordance with the maturity principle. In fact, the effect was larger than we expected, and therefore not only due to high temperature. We assume therefore that the effect of the extreme humidity was positive compared to the storage under wet jute sacks and plastic sheets used for the reference specimens.

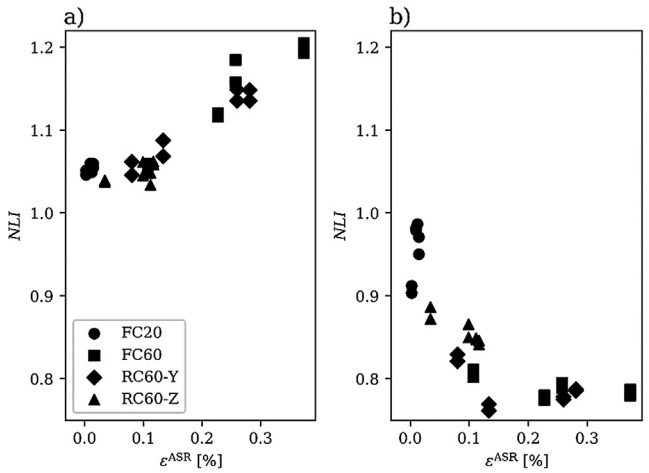

Fig. 24. NLI against expansion for a) the first load cycle, and b) as the average of the last four cycles.

The results presented in this paper, as well as those of Sanchez et al. [14] and Marzouk and Langdon [33], indicate an increase in compressive strength at early age under accelerated ASR conditions. Sanchez et al. [14] mention 0.1% expansion as the tipping point for when the compressive strength starts to decrease. Our results yield a value closer to 0.2%. In contrast, the results of both Swamy and Asali [40] and Ahmed et al. [41] not only showed no increase in compressive strength when using accelerated ASR conditions, but even a small decrease.

The greater expansion in the free directions compared to the loaded direction suggests alignment of micro cracks in the loaded direction (in line with the results in Section 3.5, which are discussed in Section 4.1). Barbosa et al. [8] report a significant loss in compressive strength, both parallel and perpendicular to the main cracking direction, in cores extracted from slab bridges in Denmark. Furthermore, they observed greater strength parallel to the main cracking direction than in the perpendicular direction. The same trends have been observed in laboratory-cast cylinders [9]. However, the opposite was observed in this study, where less compressive strength was found in the restrained direction than in the unrestrained direction. The contradictory results could be due to the presence of both macro and micro cracks in these other studies, while in the present study, no macro cracks were observed on the surface of the cores, and only micro cracks were present. To the best of our knowledge, the effect of macro cracks on the compressive strength of ordinary concrete has only been studied for (macro) cracks aligned in the longitudinal direction. A recent study by Nakamura et al. [42] found that the compressive strength decreases with crack opening. To understand the effect of macro cracks, the compressive strength perpendicular to macro cracks for ordinary concrete also needs investigation.

In addition to the alignment of cracks, concrete exposed to constant stress will creep, which might further influence the measured compressive strength. Creep and small continuous constant compressive stress over longer time periods have been reported to have a positive effect on the compressive strength due to an adaptation effect, as described for example by Bazant and Kim [43]. However, the lower compressive strength parallel to the load direction that we found is in contradiction with this positive effect. The casting direction could potentially lead to anisotropy and influence the result. Nevertheless, in our case the casting direction corresponds to the X-axis while the cylinders were drilled along the Y- and the Z-axis (Fig. 3). The casting direction should therefore have had minimal effect on the recorded compressive strength.

To sum up, the change in compressive strength due to accelerated ASR conditions is highly affected by several parameters, including the concrete mix used and the storage conditions. The results from our experiment therefore reemphasize that compressive strength is not a suitable parameter for characterizing ASR damage.

4.4. Stress-strain behaviour in compression

A more ductile behaviour, in the sense of strain at maximum stress, is apparent for the ASR-affected than for the reference cubes. Moreover, a less ductile behaviour is apparent in the cylinders drilled in the restrained direction than in the unrestrained direction of the ASR-affected concrete. The stress-strain curves in Fig. 17 make it clear that the stiffness decreases with increasing final expansion due to ASR.

In addition to the difference in compressive strength, Barbosa et al. [8] found a large difference in ductility between cores drilled parallel and perpendicular to the main cracking direction. The observed difference in ductility was one order greater than was observed in the current study, which could be explained by the extent of cracking. The macro cracks (which are easy to spot on

the samples tested by Barbosa et al. [8]) are believed to have a lot influence on the stress-strain behaviour. Because their samples were taken from bridges in service, other deteriorating mechanisms besides ASR could have been present and explain the large crack openings, e.g. freeze thaw cycles.

Fracture energy in compression is an interesting parameter for assessing damage in concrete. Fig. 20 shows that fracture energy decrease with increasing maximum transversal/lateral expansion due to ASR. The motivation for plotting the degradation in terms of lateral expansion of the cores was based on a recent study by Nakamura et al. [42] on the effect on fracture energy of longitudinal cracks and therefore transversal "crack strain", which showed that the fracture energy decrease with longitudinal crack opening. These observations are also in line with findings from theoretical micro-mechanical models in which the decrease in the fracture energy in compression is explained by the magnitude of the longitudinal micro cracks (Esposito and Hendriks [44]). It should be noted that the specimen dimensions used in this investigation (length/diameter = 2) were not ideal for avoiding the influence of the boundary conditions on the force-displacement measured in the post-peak regime; Markeset and Hillerborg [45] and Nakamura and Higai [24] have shown that the ratio should be at least 2.5. Nevertheless, the results do give some indication of the evolution of fracture energy.

As previously mentioned, the strains calculated include those deformations of the boundaries of the core. A more correct stress-strain curve could have been obtained by modifying the strain using the method proposed in Mansur et al. [46]. This method requires that the strain should be measured directly in the concrete in the pre-peak regime, e.g. by electrical resistance strain gauges glued on the concrete surface. This was not done in the current study. Future compressive stress-strain tests should include such measurement to subtract the contribution of the boundaries from the displacement measured and therefore the calculated strain.

5. Conclusions and suggestions for further research

In this investigation, concrete cubes of 230 mm side length were stored in accelerated conditions (60 °C) and compared to reference cubes stored at 20 °C. Thirty-two cores were drilled in two directions for mechanical tests: a cyclic test in compression, i.e. a stiffness damage test (SDT) and a complete stress-strain test. For one sample micro crack orientations were obtained for a plane including the restrained direction. The amount of specimens is large, but because many parameters are investigated (age, restraint, core direction and storage condition), the basis for a statistical quantification of the results is limited. Based on the results obtained in this investigation, it is confirmed that restraint affects the development of ASR in terms of expansion, mechanical properties and degree of damage, and our main conclusions are:

- Expansion due to ASR is hindered in the loaded/restrained direction, and no transfer of expansion to the unrestrained directions was observed in the present investigation. Due to the limited number of samples, more experiments should be conducted to verify the expansion behaviour of this concrete.
- The relative modulus of elasticity decreases with increasing levels of expansion due to ASR. This means that restraint, which reduces expansion, also reduces the decrease in the modulus of elasticity.
- Expansion in a given direction is correlated to the extent of micro cracks perpendicular to this direction, and the orientation and the degree of micro cracking give rise to the anisotropic stiffness degradation. Since there is no transfer of expansion to the free directions of the restrained cubes, uniaxial compressive stress helps to reduce the total damage due to ASR.
- This paper has reemphasized that the compressive strength is not suitable as a damage indicator. Compressive strength does not decrease at the same rate as the modulus of elasticity. Compressive strength might be more correlated to the lateral expansion (and therefore longitudinal micro cracking) than to the longitudinal expansion of the cores. The results found in the literature that contradict this conclusion might be explained by differences in the extent and the orientation of macro cracks.
- The damage indices (SDI, PDI and NLI) indicate a reduction of damage in the restrained direction, which corresponds well with the reduced decrease in the modulus of elasticity in the restrained direction.

If SDT is to become a reliable tool for assessing the degree of damage and correlated expansion in ASR-affected concrete structures, more testing needs to be conducted on restrained specimens in different sustained stress states and with different concrete recipes. The SDT is uniaxial and is meant to characterize the damage/expansion in the test direction. If a robust damage index is to be obtained from the SDT result – a uniaxial stress-strain relationship – it should be corrected for the effect of the existing damage/expansion in the perpendicular directions. Whether the maximum load used in the SDT should be reduced and whether the first load cycle should be discounted, as in the original test philosophy, remains an open issue for restrained experiments.

The mechanical degradation of ASR-affected concrete is most notable from the reduction of the modulus of elasticity over time. However, the modulus of elasticity cannot be regarded as a practical assessment parameter if a reference value (for unaffected concrete) is lacking. From the viewpoint of developing constitutive models, knowledge on the stiffness reduction, as well as nonlinear (and dissipative) behaviour is highly relevant. ASR-affected concrete has non-linear behaviour at low stress levels (below 40% of compressive strength), at which healthy concrete behaves in a linear elastic way. Further investigation of the (1D, 2D and 3D) stress-strain behaviour of ASR-affected concrete is needed to develop proper constitutive models.

CRediT authorship contribution statement

Simen Sørgaard Kongshaug: Conceptualization, Methodology, Software, Formal analysis, Writing - original draft, Investigation, Writing - review & editing, Visualization. **Oddbjørn Oseland:** Conceptualization, Methodology, Investigation, Writing - original draft, Visualization. **Terje Kanstad:** Conceptualization, Methodology, Writing - review & editing, Supervision, Project administration. **Max A.N. Hendriks:** Writing - review & editing, Supervision. **Eva Rodum:** Conceptualization, Methodology, Resources, Writing - review & editing, Funding acquisition. **Gro Markeset:** Writing - review & editing, Supervision.

Declaration of Competing Interest

The authors declare that they have no known competing financial interests or personal relationships that could have appeared to influence the work reported in this paper.

Acknowledgement

This study was supported by Better Bridge Maintenance (in Norwegian: Bedre Bruvedlikehold): A 5-year research and development programme, on bridges and quays, established by the Norwegian Public Roads Administration (Statens Vegvesen) in 2017. The financial support is gratefully acknowledged. The experimental work was conducted in the concrete laboratory at NTNU and SINTEF.

Appendix

Table A1
Test results for all cores.

Drilled core	Age at testing in days after casting	ε^{ASR}[%]	f_c[MPa]	$f_{c,CSS}$ [MPa]	E_{SDT}[MPa]	E_{CSS}[MPa]	G_c[N/mm]	SDI	PDI	NLI
FC20-1-Y1	50	0.002		40.3	32,483	23,001	34.5	0.087	0.101	1.046
FC20-1-Y2	50	0.002	45.1		32,691			0.085	0.101	1.051
FC20-2-Z1	85	0.014		40.8	34,246	25,603	38.5	0.065	0.045	1.059
FC20-2-Z2	85	0.014	46.7		34,298			0.068	0.059	1.055
FC20-3-Z1	120	0.010	48.1		34,951			0.053	0.027	1.060
FC20-3-Z2	120	0.010	45.8		34,269			0.055	0.032	1.060
FC20-4-Z1	162	0.012	51.6		35,767			0.049	0.017	1.049
FC20-4-Z2	162	0.012	50.3		35,380					1.072
FC60-1-Y1	50	0.107		48.1	26,183	19,822	33.1	0.148	0.205	1.048
FC60-1-Y2	50	0.107	51.8		24,717			0.161	0.219	1.060
FC60-2-Z1	85	0.227		43.6	19,521	15,150	31.7	0.194	0.230	1.120
FC60-2-Z2	85	0.227	46.7		20,181			0.186	0.221	1.116
FC60-3-Z1	120	0.257	44.1		18,650			0.196	0.217	1.185
FC60-3-Z2	120	0.257	44.2		19,607			0.180	0.213	1.158
FC60-4-Z1	162	0.373	41.5		17,772			0.203	0.229	1.205
FC60-4-Z2	162	0.373	42.3		16,655			0.200	0.205	1.193
RC60-1-Y1	50	0.080		47.2	29,222	19,971	38.8	0.136	0.195	1.062
RC60-1-Y2	50	0.080	51.5		27,493			0.138	0.196	1.046
RC60-1-Z1	50	0.034		44.6	28,740	19,699	36.9	0.100	0.114	1.038
RC60-1-Z2	50	0.034	45.8		28,365			0.110	0.136	1.040
RC60-2-Y1	85	0.133		48.2	23,122	16,151	36.1	0.188	0.262	1.088
RC60-2-Y2	85	0.133	50.4		22,149			0.192	0.276	1.069
RC60-2-Z1	85	0.112		42.8	25,522	19,493	35.7	0.127	0.153	1.048
RC60-2-Z2	85	0.112	45.6		26,356			0.122	0.156	1.034
RC60-3-Y1	120	0.259		44.7	20,527	15,290	31.4	0.190	0.231	1.135
RC60-3-Y2	120	0.259	46.6		21,415			0.188	0.235	1.149
RC60-3-Z1	120	0.117		41.5	24,839	17,884	28.9	0.126	0.152	1.059
RC60-3-Z2	120	0.117	45.0		25,525			0.128	0.162	1.062
RC60-4-Y1	162	0.281		44.1	19,348	14,828	30.8	0.185	0.214	1.135
RC60-4-Y2	162	0.281	45.8		19,251			0.191	0.219	1.148
RC60-4-Z1	162	0.099		44.0	25,547	19,198	30.8	0.116	0.133	1.045
RC60-4-Z2	162	0.099	44.8		24,219			0.128	0.140	1.061

References

[1] C. Larive. Apports combinés de l'expérimentation et de la modélisation à la compréhension de l'alcali-réaction et de ses effets mécaniques: Ecole nationale des ponts et chaussees; 1997.
[2] G. Giaccio, R. Zerbino, J. Ponce, O.R. Batic, Mechanical behavior of concretes damaged by alkali-silica reaction, Cem. Concr. Res. 38 (7) (2008) 993–1004.
[3] M. Berra, G. Faggiani, T. Mangialardi, A. Paolini, Influence of stress restraint on the expansive behaviour of concrete affected by alkali-silica reaction, Cem. Concr. Res. 40 (9) (2010) 1403–1409.
[4] H. Kagimoto, Y. Yasuda, M. Kawamura, ASR expansion, expansive pressure and cracking in concrete prisms under various degrees of restraint, Cem. Concr. Res. 59 (2014) 1–15.
[5] S. Multon, F. Toutlemonde, Effect of applied stresses on alkali–silica reaction-induced expansions, Cem. Concr. Res. 36 (5) (2006) 912–920.
[6] A.E.K. Jones, L.A. Clark, The effects of restraint on ASR expansion of reinforced concrete, Mag Concrete Res. 48 (174) (1996) 1–13.
[7] J. Liaudat, I. Carol, C.M. López, V.E. Saouma, ASR expansions in concrete under triaxial confinement, Cem. Concr. Compos. 86 (2018) 160–170.
[8] R.A. Barbosa, S.G. Hansen, K.K. Hansen, L.C. Hoang, B. Grelk, Influence of alkali-silica reaction and crack orientation on the uniaxial compressive strength of concrete cores from slab bridges, Constr. Build. Mater. 176 (2018) 440–451.
[9] G. Giaccio, M.C. Torrijos, J.M. Tobes, O.R. Batic, R. Zerbino, Development of alkali-silica reaction under compressive loading and its effects on concrete behavior, ACI Mater. J. 106 (3) (2009) 223.
[10] B.P. Gautam, D.K. Panesar, S.A. Sheikh, F.J. Vecchio, Effect of multiaxial stresses on alkali-silica reaction damage of concrete, ACI Mater. J. 114 (4) (2017) 595.
[11] P. Rivard, F. Saint-Pierre, Assessing alkali-silica reaction damage to concrete with non-destructive methods: from the lab to the field, Constr. Build. Mater. 23 (2) (2009) 902–909.
[12] T. Chrisp, P. Waldron, J. Wood, Development of a non-destructive test to quantify damage in deteriorated concrete, Mag Concrete Res. 45 (165) (1993) 247–256.
[13] L. Sanchez, B. Fournier, M. Jolin, J. Bastien, Evaluation of the stiffness damage test (SDT) as a tool for assessing damage in concrete due to ASR: test loading and output responses for concretes incorporating fine or coarse reactive aggregates, Cem. Concr. Res. 56 (2014) 213–229.
[14] L. Sanchez, B. Fournier, M. Jolin, J. Bastien, D. Mitchell, Practical use of the Stiffness Damage Test (SDT) for assessing damage in concrete infrastructure affected by alkali-silica reaction, Constr. Build. Mater. 125 (2016) 1178–1188.
[15] L. Sanchez, B. Fournier, M. Jolin, D. Mitchell, J. Bastien, Overall assessment of Alkali-Aggregate Reaction (AAR) in concretes presenting different strengths and incorporating a wide range of reactive aggregate types and natures, Cem. Concr. Res. 93 (2017) 17–31.
[16] O. Skjølsvold, E. Rodum. ASR – Field testing of surface treatment. Norwegian Public Roads Administration; 2015. Report No.: 465.
[17] J. Lindgård, P.J. Nixon, I. Borchers, B. Schouenborg, B.J. Wigum, M. Haugen, et al., The EU "PARTNER" Project—European standard tests to prevent alkali reactions in aggregates: final results and recommendations, Cem. Concr. Res. 40 (4) (2010) 611–635.
[18] Norwegian Concrete Association. Durable concrete with alkali reactive aggregates (NB21). 2008.
[19] P.J. Nixon, I. Sims. RILEM Recommendations for the prevention of damage by alkali-aggregate reactions in new concrete structures. RILEM State-of-the-Art Report; Springer: Dordrecht, The Netherlands. 2016.
[20] J. Lindgård, Alkali-silica reaction (ASR)–Performancetesting [Doctoral Thesis], Norwegian University of Science and Technology, 2013.
[21] European Standard. Cement–Part 1: Composition, specifications and conformity criteria for common cements (EN 197-1:2011). 2011.
[22] European Standard. Testing hardened concrete – Part 2: Making and curing specimens for strength tests (EN 12390-2:2009). 2009.
[23] European Standard. Eurocode 2: Design of concrete structures. Part 1-1: General rules and rules for buildings (EN 1992-1-1:2004). 2004.
[24] H. Nakamura, T. Higai. Compressive fracture energy and fracture zone length of concrete. Modeling of inelastic behavior of RC structures under seismic loads. 2001:471-87.
[25] European Standard. Testing hardened concrete – Part 3: Compressive strength of test specimens (EN-12390-3:2001). 2001.
[26] E.N. Andreassen, A.B. Elbrønd, M.T. Hasholt, The use of image analysis to quantify the orientation of cracks in concrete, in: International RILEM Conference on Materials, Systems and Structures in Civil Engineering: Rilem publications, 2016, pp. 1–10.
[27] H.X. Wen. Prediction of structural effects in concrete affected by alkali-aggregate reaction [PhD Thesis] 1993.
[28] C. Gravel, G. Ballivy, Khayat K, Quirion M, Lachemi M, editors. Expansion of AAR Concrete under Triaxial Stresses: Simulation with Instrumented Concrete Block. In Proceedings of the the 11th International Conference on Alkali Aggregate Reaction; 2000; Québec, Canada.

[29] T.M.A. Ahmed, E. Burley, S.R. Rigden, The effect of alkali—silica reaction on the fatigue behaviour of plain concrete tested in compression, indirect tension and flexure, Mag Concrete Res. 51 (6) (1999) 375–390.
[30] C.F. Dunant, K.L. Scrivener, Effects of uniaxial stress on alkali–silica reaction induced expansion of concrete, Cem. Concr. Res. 42 (3) (2012) 567–576.
[31] X.X. Gao, S. Multon, M. Cyr, A. Sellier, Alkali–silica reaction (ASR) expansion: pessimum effect versus scale effect, Cem. Concr. Res. 44 (2013) 25–33.
[32] N. Smaoui, M.-A. Bérubé, B. Fournier, B. Bissonnette, Influence of specimen geometry, orientation of casting plane, and mode of concrete consolidation on expansion due to ASR, Cem. Concr. Aggregates 26 (2) (2004) 1–13.
[33] H. Marzouk, S. Langdon, The effect of alkali-aggregate reactivity on the mechanical properties of high and normal strength concrete, Cem. Concr. Compos. 25 (4–5) (2003) 549–556.
[34] A.E.K. Jones, L.A. Clark, The effects of ASR on the properties of concrete and the implications for assessment, Eng. Struct. 20 (9) (1998) 785–791.
[35] R. Esposito, C. Anaç, M.A. Hendriks, O. Çopuroğlu, Influence of the alkali-silica reaction on the mechanical degradation of concrete, J. Mater. Civ. Eng. 28 (6) (2016) 04016007.
[36] B. Capra, A. Sellier, Orthotropic modelling of alkali-aggregate reaction in concrete structures: numerical simulations, Mech. Mater. 35 (8) (2003) 817–830.
[37] É. Grimal, A. Sellier, Y. Le Pape, É. Bourdarot, Creep, shrinkage, and anisotropic damage in alkali-aggregate reaction swelling mechanism-Part I: a constitutive model, ACI Mater. J. 105 (3) (2008) 227.
[38] P. Morenon, S. Multon, A. Sellier, E. Grimal, F. Hamon, E. Bourdarot, Impact of stresses and restraints on ASR expansion, Constr. Build. Mater. 140 (2017) 58–74.
[39] R. Balendran, W. Martin-Buades, The influence of high temperature curing on the compressive, tensile and flexural strength of pulverized fuel ash concrete, Build. Environ. 35 (5) (2000) 415–423.
[40] R. Swamy, M. Al-Asali, Engineering properties of concrete affected by alkali-silica reaction, Mater. J. 85 (5) (1988) 367–374.
[41] T. Ahmed, E. Burley, S. Rigden, A.I. Abu-Tair, The effect of alkali reactivity on the mechanical properties of concrete, Constr. Build. Mater. 17 (2) (2003) 123–144.
[42] T.N. Hikaru Nakamuraa, Taito Miuraa, Sushanta Roya. Experimental investigation of compressive strength and compressive fracture energy of longitudinally cracked concrete, Cem. Concr. Compos. 93 (2018;Volume) 1–18.
[43] Z.P. Bazant, S.S. Kim, Nonlinear creep of concrete-adaptation and flow, ASCE J. Eng. Mech. Div. 105 (3) (1979) 429–446.
[44] R. Esposito, M.A. Hendriks, A multiscale micromechanical approach to model the deteriorating impact of alkali-silica reaction on concrete, Cem. Concr. Compos. 70 (2016) 139–152.
[45] G. Markeset, A. Hillerborg, Softening of concrete in compression—localization and size effects, Cem. Concr. Res. 25 (4) (1995) 702–708.
[46] M. Mansur, T. Wee, M. Chin, Derivation of the complete stress-strain curves for concrete in compression, Mag. Concr. Res. 47 (173) (1995) 285–290.